Detecting sub-glacial aquifers in the north polar layered deposits with Mars Express/MARSIS

W. M. Farrell,[1] J. J. Plaut,[2] D. A. Gurnett,[3] and G. Picardi[4]

Received 19 January 2005; revised 9 April 2005; accepted 29 April 2005; published 10 June 2005.

[1] The penetration of the MARSIS radar signal into the polar ice mass is modeled to determine the capability of the instrument to locate sub-glacial aquifers. As a ground penetrating radar, the orbiting MARSIS transmits a signal >1 W between 1–5 MHz. In this work we will investigate the effect of ice reflective and conductive losses on the radar-detection of subsurface aquifers using an MGS MOC profile of the ice layering. We find that a basal lake located ~2.5 km below the surface is at the limit of detectability.
Citation: Farrell, W. M., J. J. Plaut, D. A. Gurnett, and G. Picardi (2005), Detecting sub-glacial aquifers in the north polar layered deposits with Mars Express/MARSIS, *Geophys. Res. Lett.*, *32*, L11204, doi:10.1029/2005GL022488.

1. Introduction

[2] A primary science goal of the Mars Exploration Program (MEP) is the search for subsurface water. The Mars Express/Mars Advanced Radar for Subsurface and Ionospheric Sounding (MEX/MARSIS) is a subsurface radio sounding system currently in Mars orbit that can transmit and receive signals in a range between 0.1–5.5 MHz with peak power levels near 10 W. The primary science goal of the investigation is to map the distribution of water, both liquid and solid form, in the upper portions of Mar's crust. The anticipated probing depth of the subsurface sounder is between 0.1–5 km, depending upon conditions. This depth range is fairly broad, and it would be desirable to quantify more exactly the expected probing depth in the polar ice mass regions.

[3] Basal lakes are defined as water reservoirs formed at the underside of an ice mass. For example, such lakes are found at the ice/rock interface under the Antarctic ice cap [*Oswald and Robin*, 1973]. *Clifford* [1987, 1993] has described the possibility of such basal lake formation under the Martian polar cap (defined as the remnant water ice cap and underlying dusty-ice polar layered deposits or PLD) via melting from ice insulation effects, local geothermal hot spots, or heat-generating glacial sliding. Ice cap basal melting may be an important process in the Martian hydrological cycle [*Clifford*, 1993, 2003]. Such melts may feed a quasi-global water table located many kilometers below the surface.

[4] Basal lakes represent a key target for MARSIS during its Northern low-perigee polar overpasses in April–May 2005. There are significant periods when the MEX periapsis is over the nighttime Martian north pole region. During these times, ionosphere attenuation is expected to be minimized and a direct radio sounding of the polar ice caps is possible. However, the ability to return a signal from a deep aquifer is a strong function of a number of variables, including overlying ice composition, which is currently unknown. In this letter, we will examine the feasibility of detecting the ice cap base given various cap top-layer compositions.

2. MEX and MARSIS Description

[5] Mars Express was successfully launched on 2 June 2003 and completed a 24 December 2003 orbit insertion about the planet. The anticipated mission is 1 Martian year (687 days). The 86° eccentric orbit ranges from a periapsis of 279 km to an apoapsis of 11634 km. The initial latitude of periapsis is near the equator and this periapsis latitude will drift by about 0.5 degrees per sol. Over the course of the mission, the periapsis location will migrate over both poles during favorable periods when they are unlit (i.e., the intervening ionosphere density is low). The ideal date for north polar sounding is April–May 2005.

[6] The MARSIS instrument consists of a 40-m antenna transmitter/receiver system. The antennae have yet to be deployed because initial post-launch tests suggested attaching hinges might become overstressed upon deployment. Further studies suggest this mechanical issue is not as serious as initially believed, and deployment is tentatively scheduled for March 2005. In subsurface sounding mode, the transmitter emits a 1 MHz bandwidth pulse in 4 distinct bands: 1.3–2.3 MHz, 2.5–3.5 MHz, 3.5–4.5 MHz, and 4.5–5.5, MHz. The 40-m antenna will have a resonance frequency at $f_{res} \sim 3.75$ MHz, and transmission near this band will be emitted at peak powers (5–10 W). Below this resonance, transmission power is less efficient which is a natural consequence of radio transmission via short dipole radiators [*Calvert et al.*, 1995].

3. Polar Layered Deposit Profiles

[7] In order to assess the effect of the overlying ice on aquifer detection, we examine an MGS/MOC image of the PLD shown in Figure 1 (M. C. Malin et al., MOC extended mission view of the north polar layers, NASA's Planetary Photojournal, available at http://photojournal.jpl.nasa.gov/). As described by Malin et al., this revealing image shows a 14.5 km region of exposed terrain (a scarp) along Chasma Boreale, showing the internal layering structure of the

[1]NASA Goddard Space Flight Center, Greenbelt, Maryland, USA.
[2]Jet Propulsion Laboratory, Pasadena, California, USA.
[3]Department of Physics and Astronomy, University of Iowa, Iowa City, Iowa, USA.
[4]INFO-COM Department, University of Rome, Rome, Italy.

0094-8276/05/2005GL022488$05.00

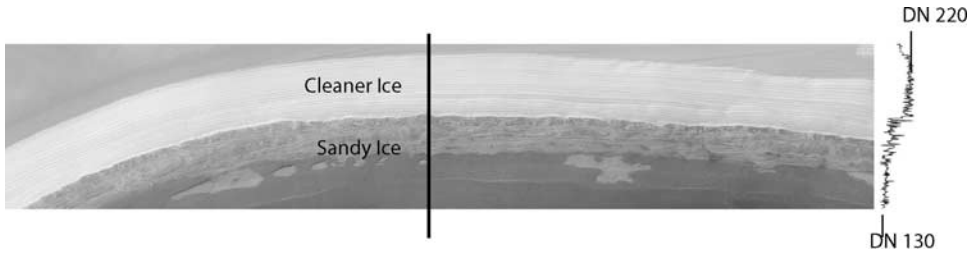

Figure 1. An MGS/MOC image showing a scarp along Chasma Boreale (http://photojournal.jpl.nasa.gov/). Our study examines the exposed vertical terrain along the dark line, and the profile of relative brightness at this location is shown in the adjacent line plot. The association of data number and radiance scale is approximately linear, suggesting a factor of two reduction in brightness from top to bottom layers.

deposit. The brighter top region is suggestive of a set of ice/snow layers with a relatively low concentration of imbedded dust impurities, while the darker terrain underneath appears to be set of layers with a large amount of entrained sand (http://photojournal.jpl.nasa.gov/). This deeper sandy ice layer is shown on other images to be the source of a polar sand dune fields created by wind erosion. Via scaling, we assume the height of the PLD layering is about ~2.5 km (assuming little/no foreshortening). The unique element of this image is that the composition of the layering is pronounced, with relatively clean ice layers over "dirty" sandy ice layers.

[8] We focused on a vertical profile of the layering indicated by the line plot to the right in Figure 1. The vertical profile is that of relative optical brightness, with larger values indicative of relatively "clean" icy layering (whiter) and smaller values indicative of sandy ice layering (darker). In order to understand wave propagation effects though such layering, both relative permittivity and conductivity profiles are required. While these profiles do not exist, we used the relative brightness profile as a proxy, indicating the concentration of dust in the ice: We assume that permittivity values vary directly with brightness values, with upper ice layer brightness values (near DN 220 counts) being given a relative permittivity, ε, of 4 (typical value for ice) and the nominal lower sandy ice later brightness values (near DN 130 counts) being assigned a permittivity of 5 (typical of sand). All other values are interpolated between these two values. We note that these count values scale approximately linearly with radiance. Hence, there appears to be nearly a factor of two change in brightness between the top and bottom layers.

[9] The conductivity is derived in a similar way, but using two steps. First, we assume the relative reflectivity of the ice layers is a function of the dust fractional volumetric concentration, n_{dust}, (i.e., the dust-to-ice volume ratio). Pure ice has a visible reflectivity near 0.5, but concentrations of medium-to-dark albedo dust reduce the effective reflectance from this ideal value [*Clark and Lucey*, 1984]. We thus assume the reduction in reflectance from pure ice scales with the exposed "clean" ice area. Given these assumptions, we presume to account for the approximate factor of two reduction in radiance between top and bottom ice layers in Figure 1 by assigning $n_{dust} \sim 0.1$ to the upper "clean" ice layers (90% exposed ice) which is assumed to reduce the reflectance to 0.45 (90% of pure ice value), and assigning $n_{dust} \sim 0.5$ in the lower darker sandy ice layers (50% exposed ice) which is assumed to reduce the reflectance to 0.25 (50% of pure ice value). Linear interpolation for other brightness values provides a conversion of profiles from optical brightness to dust concentration. Second, Figure 2 of *Chyba et al.* [1998] shows the dependency of conductivity with dust concentration and ice temperature (see Appendix) and this information is then used to convert the dust concentration profile into a conductivity profile $\sigma = \sigma(z, n_{dust}, T_{ice})$. For our initial calculations, we assume that the north PLD temperature ranges from 273°K at its base (warm enough to melt ice to create basal lake) to ~205°K at the surface [*Clifford*, 1987, 1993] and varies linearly with depth (as suggested in equation (16) of Chyba et al., the function is actually an exponential of a log, but results in a quasi-linear variation). Thus, with this approach, each brightness value at point z along the profile can be converted via the model to a permittivity and conductivity value, and these are displayed in Figure 2. The approach is non-unique since the actual reflectance of dusty ice is highly dependent upon specific composition/mineralogy of the dust grains, which we do not know [*Clark and Lucey*, 1984]. However, the highly-revealing image in

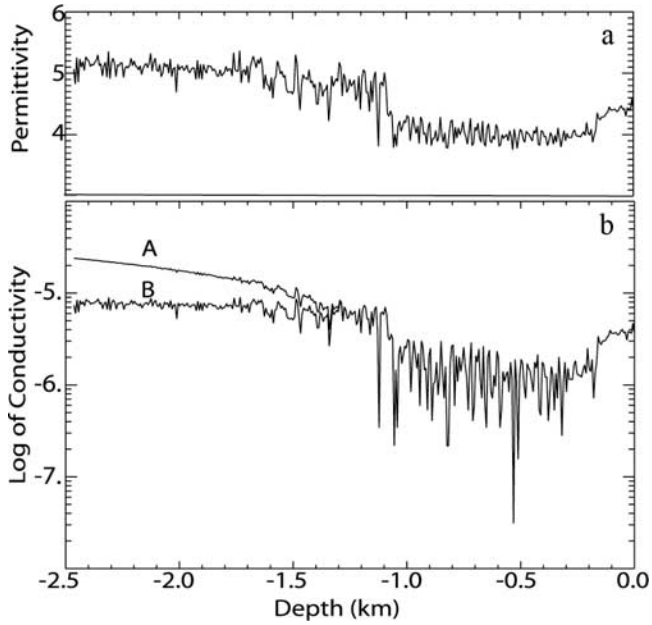

Figure 2. Relative permittivity and conductivity using the profile in Figure 1. The conversion of relative brightness values to electrical values is described in the text.

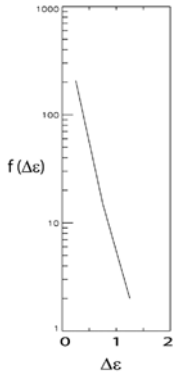

Figure 3. The number distribution of interfaces as a function of change in permittivity.

Figure 1, particularly the very sharp contrast between upper and lower layers, gives insight into the dust/soil concentration of the PLD that allows a gross approximation of the electrical properties of the medium. The previous work regarding "dirty" ice conductivity, including its temperature dependence with the addition of impurities/soil by *Chyba et al.* [1998] is integrated into the model.

[10] Figure 2b, curve A shows the conductivity profile for a "warm" base of 273°K and surface temperature of 205°K. Case B considers a "cold" PLD, this being isothermal and set at the exterior surface temperature of 205°K. In this second case, the cap is assumed to not warm from below via the insulation effect described by *Clifford* [1987, 1993]. Note that the conductivity profile differs substantially between the two cases, with the warm case yielding larger values of σ at lower depth/higher temperature by nearly a factor of 3 over the cold isothermal case.

4. Return Electric Field and System Losses

[11] The return electric field back to MARSIS can be described by the expression:

$$E_{ret}(r) \sim D(r)\tau(\Delta\varepsilon)A(f,\sigma,d)I(f,fp,n) \quad (1)$$

where D is the divergence of the wave propagating from the point source transmitter, τ is the transmission coefficient through N layers of relative dielectric change $\Delta\varepsilon$, A is the medium conductive attenuation, and I is the ionospheric attenuation which is dependent upon wave frequency, f, ionosphere plasma frequency, f_p, and neutral density, n. The variable r is the distance between the spacecraft and surface. In April–May 2005, when MARSIS perigee passes over the northern polar region, the pole will be in nighttime unlit conditions, with a relatively low ionospheric plasma density [*Zhang et al.*, 1990]. Consequently, for transmissions near 4 MHz, we assume f is well above the local fp, and factor I is near unity.

[12] The divergence factor is

$$D(r) = (377\,P)^{1/2}/2(2\pi)^{1/2}(r+d) \sim (377\,P)^{1/2}/2(2\pi)^{1/2}r \quad (2)$$

where we assume perfect reflection from a flat conducting plate located at a distance $d \ll r$ below the surface. Without any subsurface losses (τ and A equal to unity), a 4 MHz transmitted power pulse of 5 W at a radial distance of 275 km will yield an $E_{ret} \sim 31$ μV/m. The noise level of the receiver is assumed to be cosmic background at $E_{noise} \sim 5$ μV/m [*Farrell et al.*, 2004]. Hence, under ideal circumstances a ~16 dB signal should be obtained above the noise level from a highly reflective aquifer/basal lake. However, if the overlying PLD gives rise to −16 dB of reflective (τ) or conductive (A) losses over the two-way path, or −8 dB of one-way path loss, then the return signal drops below the noise level and the aquifer may becomes undetectable. Onboard spectral integration techniques may provide an added 20 dB of additional sensitivity, increasing the detection threshold to 36 dB (or 18 dB for one-way loss).

[13] Reflective losses, or those losses associated with wave penetration through interfaces of differing dielectric, are lumped into factor τ. Assuming a small change in relative permittivity across an interface separating region 1 and 2, $\varepsilon_2 = \varepsilon_1 + \Delta\varepsilon$, the wave reflectance can be rewritten as

$$R = \left(\varepsilon_1^{1/2} - \varepsilon_2^{1/2}\right)^2 / \left(\varepsilon_1^{1/2} + \varepsilon_2^{1/2}\right)^2 \sim \Delta\varepsilon^2/16\varepsilon_1^2 \quad (3)$$

and transmission coefficient through N identical layers as

$$T^N = (1-R)^N = \left(1 - \Delta\varepsilon^2/16\varepsilon_1^2\right)^N \sim \left(1 - N\,\Delta\varepsilon^2/16\varepsilon_1^2\right) \quad (4)$$

For transmission through N_i layers, with each N_i having a different differential permittivity, $\Delta\varepsilon_i$, the expression becomes

$$T^N \sim 1 - \sum N_i\Delta\varepsilon_i^2/16\varepsilon_1^2 \sim 1 - \int f(\Delta\varepsilon)\Delta\varepsilon^2 d(\Delta\varepsilon)/16\langle\varepsilon\rangle^2 \quad (5)$$

where $f(\Delta\varepsilon)$ is the number distribution of interfaces between $\varepsilon - \Delta\varepsilon/2$ and $\varepsilon + \Delta\varepsilon/2$ such that $N = \int f(\Delta\varepsilon)\, d(\Delta\varepsilon)$. The variable $\langle\varepsilon\rangle$ is the average permittivity value (which for small changes is approximately ε_1). The factor $\tau = \sqrt{T^N}$. The quantity $f(\Delta\varepsilon)$ required to obtain τ is derivable via the $\varepsilon(z)$ profile in Figure 2a. To determine $\Delta\varepsilon$, we identified the local maxima and minima in the ε profile shown in Figure 2a, and calculated the $\Delta\varepsilon$ between each maximum/minimum pair. There were a total of N = 224 interfaces, and the profile of $f(\Delta\varepsilon)$ is shown in Figure 3 for the case in Figure 2a.

[14] The attenuation factor, A, varies as $\exp(-n_i\omega\, d/c)$, where n_i is the imaginary portion of the index of refraction, d is the layer depth and ω is the wave frequency. As long as $\sigma < \varepsilon\varepsilon_o\omega$ or $\sigma < 1 \times 10^{-3}$ S/m at 4 MHz, the imaginary part of the index of refraction is $n_i \sim \sigma/2\varepsilon_o\omega\varepsilon^{1/2}$. For a

Table 1. Results From Model Runs

	ε_{top}	ε_{bot}	n_{top}	n_{bot}	T_{surf} (°K)	T_{base}(°K)	τ (dB)[a]	A (dB)[a]
A	4	5	0.1	0.5	205	273	−0.16[b]	−15.9[b]
B	4	5	0.1	0.5	205	205	−0.16[c]	−8.5[c]
C	4	5	0.2	0.6	205	273	−0.16	−17.9
D	4	5	0.3	0.7	205	273	−0.16	−20.0
E	12	5	0.1	0.5	205	273	−2.7	−16.1
F	4	4.5	0.1	0.5	205	273	−0.11	−16.6
G	4	3	0.1	0.5	205	273	−0.29	−20.2

[a]One-way loss.
[b]Conductivity profile applied shown in Figure 2b, Curve A.
[c]Conductivity profile applied shown in Figure 2b, Curve B.

number of layers each of size d_i with differing conductivity, σ_i, the attenuation can be expressed as

$$A = \exp\left(-\sum \sigma_i d_i / 2\varepsilon_o \varepsilon_i^{1/2} c\right) = \exp\left(-(2\varepsilon_o c)^{-1} \int \sigma(z)\varepsilon(z)^{-1/2} dz\right) \quad (6)$$

with $\varepsilon(z)$ and $\sigma(z)$ provided in Figures 2a and 2b respectively.

[15] Table 1 shows the results of the calculation. Case A is run for the situation of the top white ice layers at n = 0.1 and lower sandy ice layers at n = 0.5 ice/soil concentrations respectively, and a linear variation in temperature in the layering from 205°K at the surface to 273°K at the base (conductivity profile is Figure 2b, curve A). Case B is run for the situation where the PLD is isothermal at 205°K (conductivity profile is Figure 2b, curve B). Other cases are also examined.

5. Conclusions

[16] The reflective losses (τ) in the PLD are minimal. However, the conductive losses (A) for a warmed PLD (Case A) are substantial, being ~16 dB in one-way or ~32 dB in two way propagation. Since the ideal (lossless) two-way system signal-to-noise is ~16 dB (and 36 dB with spectral integration), the modeling suggests that an aquifer located at the base of PLD layer will be at signal levels well below the cosmic background level and will require spectral integration for detection. Conversely, if the PLD remains isothermal and cold (Case B), deeper penetration is possible, with only ~17 dB of two-way loss at the same depth, a situation just at the limit of direct detectability. However, because the PLD is cold, basal lakes would not be expected in this case.

[17] The results suggest an ironic situation where a warmed polar base (either by insulation or local geothermal heat sources) will create basal melting but also increase the overlying ice temperature (and conductive path loss), thereby making aquifer detection increasingly difficult. The model is not unique or complete: Other factors like surface scattering (not included) [*Picardi et al.*, 2004] will add further losses while lower-than-modeled dust concentrations may improve the detectability. A possible highly-attenuating meteoric layer near 80 km altitude is not considered herein [*Pesnell and Grebowsky*, 2000; *Witasse et al.*, 2001]. Also, any unfrozen water mixed with the ice will increase conductivity/attenuation beyond model values. We have attempted to connect the very revealing MOC image and its suggestive dust/ice concentration with modern "dirty ice" conductivity models. Admittedly, the conversion of the relative optical brightness profile into electrical parameters yields a non-unique solution, but still provides new insights into MARSIS system losses and their affect on polar aquifer detection, particularly when considering the overlying dirty ice concentrations and temperatures. The search for these basal lakes with the newly-deployed MARSIS is an exciting possibility eagerly anticipated for April 05, and the calculations herein can be verified experimentally at that time.

Appendix A: Model of Ice Conductivity

[18] Figure 2 of *Chyba et al.* [1998] shows the 60 MHz attenuation in ice with lunar soil mixtures of fractional volume of n_{dust} = 0.1, and 0.5 as a function of temperature. This attenuation can be converted to conductivity via equation (1) of Chyba et al. General formalism representing these temperature-dependent conductivities were applied in our model using $\sigma(n_{dust}) = 14 \times 10^{-6}\, n_{dust}$ for temperatures T < 240°K and $\sigma(n_{dust}, T) = \sigma(n_{dust}) + \alpha(\sigma(n_{dust}))\, T$ for 240°K < T < 273°K, where $\alpha(\sigma(n_{dust})) = (\sigma_h - \sigma(n_{dust}))/\Delta T$, with $\sigma_h = 2.4 \times 10^{-5}$ S/m and ΔT = 273°K − 240°K = 33°K.

[19] **Acknowledgments.** This research was funded under the auspices of a MEX/MARSIS Participating Scientist grant from Mars Program Office at NASA HQ. We also thank Tom Watters for a helpful review and providing us with some understanding of the image and associated processing. We also thank Yanbin Xu for a careful reading of the manuscript.

References

Calvert, W., et al. (1995), The feasibility of radio sounding in the magnetosphere, *Radio Sci.*, *30*, 1577.

Chyba, C. F., S. J. Ostro, and B. C. Edwards (1998), Radar detectability of a subsurface ocean on Europa, *Icarus*, *134*, 292.

Clark, R. N., and P. G. Lucey (1984), Spectral properites of ice-particulate mixtures and implications for remote sensing, *J. Geophys. Res.*, *89*, 6341–6348.

Clifford, S. M. (1987), Polar basal melting on Mars, *J. Geophys. Res.*, *92*, 9135.

Clifford, S. M. (1993), A model for the hydrological and climatic behavior of water on Mars, *J. Geophys. Res.*, *98*, 10,973.

Clifford, S. M. (2003), The iceball next door, *Sky Telescope*, *106*, 30.

Farrell, W. M., et al. (2004), Mars Express MARSIS radar: A prediction of the effect of overlying ice on detecting polar basal lakes and inter-glacial aquifers, *NASA/TM-2004-212749*.

Oswald, G. K. A., and G. Robin (1973), Lakes beneath the Antarctic ice sheet, *Nature*, *245*, 251.

Pesnell, W. D., and J. Grebowsky (2000), Meteoric magnesium ions in the Martian atmosphere, *J. Geophys. Res.*, *105*, 1695.

Picardi, G., et al. (2004), Performance and surface scattering models for the Mars Advanced Radar for Subsurface and Ionosphere Sounding (MARSIS), *Planet. Space Sci.*, *52*, 149.

Witasse, O., J.-F. Nouvel, J.-P. Lebreton, and W. Kofman (2001), HF radio wave attenuation due to a meteoric layer in the atmosphere of Mars, *Geophys. Res. Lett.*, *28*, 3039.

Zhang, H. M., J. G. Luhmann, and A. J. Kliore (1990), An observational study of the nightside ionospheres of Mars and Venus with radio occultation methods, *J. Geophys. Res.*, *95*, 17,095.

W. M. Farrell, NASA Goddard Space Flight Center, Greenbelt, MD 20771, USA. (william.farrell@gsfc.nasa.gov)

D. A. Gurnett, Department of Physics and Astronomy, University of Iowa, Iowa City, IA 52242, USA.

G. Picardi, INFO-COM Department, University of Rome, Rome, Italy.

J. J. Plaut, Jet Propulsion Laboratory, Pasadena, CA 91109, USA.